(Article begins on next page)

Laplacian-Based Focus Measure Allows Rapid Focus Estimation of Annular Regions in Gray-Scale Images

1st Ettore Masetti
Department of Engineering "Enzo Ferrari"
University of Modena and Reggio Emilia
Via Vivarelli 10, 41125, Modena, Italy
ettore.masetti@unimore.it

2nd Mario Ettore Giardini
Department of Biomedical Engineering
University of Strathclyde
Wolfson Centre, 106 Rottenrow, Glasgow G4 0NW
mario.giardini@strath.ac.uk

3rd Marco Ruggeri
Bascom Palmer Eye Institute - Ophthalmology
University of Miami - Miller School of Medicine
900 NW 17th St, Miami, FL 33136, Stati Uniti
MRuggeri@med.miami.edu

4th Luigi Rovati
Department of Engineering "Enzo Ferrari"
University of Modena and Reggio Emilia
Via Vivarelli 10, 41125, Modena, Italy
luigi.rovati@unimore.it

Abstract—Important ophthalmic imaging techniques, such as fundus camera imaging, utilize light sources that need to be focused on an annular section of an eye surface. In order to be performed dynamically, this requires real-time control of the focus plane of the illumination optics. When considering adaptive focusing in ophthalmic instruments, liquid lenses represent the best compromise in terms of tunability, tuning range, compactness, numerical aperture, and speed. In recent years, several compact eye imaging devices using liquid lenses have been described in the literature. These would benefit from low computational complexity algorithms for adaptive local auto-focus on an annular region, to allow the illumination optics to be controlled by low-cost and low-power electronics. In this paper, we propose a novel radial-focus evaluation method based on a revised version of a more traditional Laplacian-based focus estimator. This radial focus evaluation is targeted to focusing annular sections of an image, with the advantage of a drastic reduction of computational complexity.

Index Terms—focus estimator, liquid lenses, focus quality, auto-focusing, illumination optics, imaging, optics

I. INTRODUCTION

Automated focusing technology is a crucial part of adaptive imaging systems. Autofocusing systems are usually composed of an actively adjustable optical imaging setup, an illumination optics, and a digital image capture unit, such as a digital camera. The system, if appropriately designed, allows for real-time automated focusing, with consequent advantages in imaging time-variant targets, e.g., moving objects.

Conventional active focusing systems are based on glass lenses displaced by motors. The imaging system focal length, focus plane, and aperture can be modified depending on the required field of view, depth of field, spatial resolution and focus distance [1]. Despite being more versatile and practical than a mono-focal lens, the motorized zoom lenses' bulkiness limits their use when designing highly integrated systems.

On the other end of autofocus system complexity, driven by the market of mobile camera modules with autofocus, where cost and size aspects are crucial, Voice-Coil Motors (VCMs) with spring return are, arguably, the smallest, least expensive, most straightforward, and most widely available autofocus devices to date. The lens position is set by balancing VCM and spring forces during movement. The devices are gearless, and the focussing process is highly repeatable. If no focusing is necessary, the spring returns the lens to its infinite-focus position using no power. Its mechanics are affordable and durable. However, the compactness given by VCMs inherently limits the system's numerical aperture, which makes them ineffective for those ophthalmic imaging devices, such as indirect ophthalmoscopes and autorefractors, where high numerical aperture is essential.

A possible alternative to VCMs is given by liquid optical lenses with electrically controllable focal lengths. With respect to traditional focusing systems, based on lenses displaced by electromagnetic or electrostatic motors, these devices reduce complexity, size, weight, response time, and power consumption. Indeed, an electrically tunable lens is a refractive element with a focal length that can vary without shift of the lens plane with respect to the sensor plane. In practice, the interface between two immiscible liquids with differing refractive indices, or a liquid enclosed in a highly flexible membrane, can be exploited to create liquid lenses with adjustable focal lengths [2]. The diameters can range in the tens of mm even in commercial devices. Therefore, liquid lenses represent an excellent compromise when large numerical aperture, compactness, speed, and wide tuning range are needed.

The use of liquid lenses is well-established in ophthalmic instrumentation [3]–[5] when, due to ergonomics and/or transportability requirements, significant numerical aperture, tun-

ability, and compactness, are simultaneously needed. However, because of the nature of singlet lenses, the Petzval field curvature prevents the possibility of imaging a flat surface normal to the optical axis (target) onto a flat surface (sensor). An accessory optical element (field flattener) may be used to rectify the field curvature, but this adds bulk and complexity. Designs can also include curved focal planes, as in the human eye, where the retina is an approximately spherical surface that matches the field curvature of the lens. However, this solution is not feasible when using conventional low-cost digital sensors, which are planar. So, unavoidably, a flat target in front of a singlet-based imaging system cannot be completely focused in all its areas, and only annular sections concentric to the optical axis, which typically intercepts the sensor in its center, will be in focus at any one time.

A fundamental aspect when designing an auto-focusing system is the development of an auto-focusing algorithm to correctly drive the focus adjustment device. In portable and compact ophthalmic instruments, where the focusing needs to be based only on the image captured by the sensor, and where the computational power is limited to that of the simplest possible microcontroller compatible with the application, the development of focus estimation procedures with the lowest computational weight is critical. Given the human eye's radial symmetry, the most common lighting systems for imaging the back of the eye focus the light on an annular region on the iris plane, and this makes focus estimations dedicated to focusing specific annular sections of the image of great interest. This paper proposes a focus estimation procedure that exploits radial symmetry to drastically reduce the computational complexity with respect to standard focus estimators. This algorithm is, in principle, suitable for directing the liquid lens focal power to obtain the highest degree of focus in specific annular sections of the imaging area.

This work is not intended to analyze the lens performance but to propose a focus estimation procedure capable of describing the radial degree of focus, still offering low computational complexity. Amongst several state-of-the-art sharpness metrics, the proposed approach is based on a custom radial Laplacian variance technique, which we applied to 1366x1366 px grey-scale images. In Section II, we present the state of the art of sharpness metrics, Section III demonstrates our annular auto-focusing algorithm, in Section IV, the proposed approach is applied to images acquired through a standard imaging system, and in Section V, paper conclusions are drawn.

II. Theoretical Background of Focus estimation Operators

The degree of focus of an image, or of a specific image region, can be evaluated using a broad range of algorithms and, indeed, the literature proposes a wide range of approaches, that can be broadly grouped into 3 families: derivative-based, statistical-based, and Discrete Cosine Transform (DCT)-based. [6] The derivative-based family can in turn be divided into first-order (gradient-based) or second-order (Laplacian-based) operators. These methods evaluate the edge sharpness present in the image, under the assumption that focused images present sharper edges than blurred ones. The second group applies statistical operators to the image to gather contrast descriptors, which can be correlated to the degree of focus. The last family is based on the higher content of high-spatial-frequency texture of focused images with respect to non-focused ones, exploiting the DCT coefficients to build an estimator of the image focus from the spatial frequency components. [7]

To investigate the image's local and global focus, we chose the approach with the lowest computational complexity, designing an estimator built on the analysis of the variance of the Laplacian. [8] To a certain extent, this family of algorithms mimics DCT-based operators, as it considers the range of spatial frequencies in the image, considering the image in-focus if there are a large number of high frequencies. However, the recursive nature of the FFT algorithm makes Laplacian-based approaches computationally much lighter.

In the following, we briefly consider the Laplacian operator and its variance as a powerful image-focus metric.

A. Laplacian Operator

The Laplacian approach to a focus metric is based on the application of the Laplacian operator to a 2-dimensional greyscale image, described as a bidimensional distribution of intensity $I(x,y)$:

$$\nabla \cdot \nabla I = \nabla^2 I = \frac{\partial^2 I}{\partial x^2} + \frac{\partial^2 I}{\partial y^2}. \tag{1}$$

In other words, the Laplacian of the image is defined by the sum of unmixed second partial derivatives.

The Laplacian of I can also be seen as the trace of the Hessian function $\nabla^2 I = \text{Tr}[H(I)]$. Thanks to the invariance of the trace of a matrix to the change of basis, the Laplacian operator can be conveniently rewritten in polar coordinates:

$$\nabla^2 I = \frac{\partial^2 I}{\partial r^2} + \frac{1}{r}\frac{\partial I}{\partial r} + \frac{1}{r^2}\frac{\partial^2 I}{\partial \phi^2}. \tag{2}$$

This result can be particularly helpful when performing a focus analysis in polar coordinates.

B. Variance of the Laplacian Operator

The Laplacian highlights regions of an image containing rapid intensity changes. In other words as, on sharp edges, the intensity changes rapidly in a small region, the Laplacian operator can be efficiently employed as edge detector. We note that non-sharp features are present in all images, while sharp features are present in focused images only. Therefore, an image with high variance of the Laplacian operator over the image is characterized by a wide distribution of sharp and non-sharp features, which indicates a higher degree of focus. Conversely, an image with low variance is characterized by a reduced spread of feature sharpness, which corresponds to a negligible amount of sharp edges in the image, i.e., a defocused image. Therefore, the variance of the Laplacian of

an image can be a useful metric to quantify the degree of focus, and can be computed as:

$$\phi_{i,j} = \frac{1}{\#\Omega(x,y)} \sum_{(i,j) \in \Omega(x,y)} \left(\nabla^2 I(i,j) - \overline{\nabla^2 I} \right)^2, \quad (3)$$

where $\Omega(x,y)$ is defined as every pixel neighborhood, $\overline{\nabla^2 I}$ is the average value of the image Laplacian over $\Omega(x,y)$ and $\#\Omega(x,y)$ is the cardinality of $\Omega(x,y)$. A smart selection of the neighborhood region $\Omega(x,y)$ can be extremely useful to perform different types of focus analysis. For instance, if $\Omega(x,y)$ is extended to the entire image $I(x,y)$ area, the obtained variance value can be used to compute the overall image degree of focus.

III. RADIAL FOCUS EVALUATION METHOD

A. Motivation and Requirements

The goal of the proposed method is to perform a radial focus analysis on grey-scale images. Given that, we are searching for a radial focus, effectively only a circular region of the image is analyzed. The method can therefore be described for square images without loss of generality. Let us consider images with a resolution (W_0, H_0) px. The radial analysis consists in considering the image focus uniformity starting from the image center $(W_0/2, H_0/2)$ up to the maximum radius inscribed in the image.

As a reminder, the motivation of this approach is that the majority of imaging systems present an axial symmetry around the axis of the acquisition sensor and that we are optimizing the measurement to describe the focus of annular features around the image center. Therefore, a radial focus map analysis is the most advantageous when the system presents this type of symmetry. The method described in this paper aims to address the definition of a focus estimator for the annular focus/defocus regions originating on the sensor plane from field curvature introduced, e.g., by a liquid lens.

The proposed algorithm is implemented using the Python 3.9 programming language and the OpenCV 4.6 package for image processing [9]. Data manipulation is performed using the NumPy package, [10] which is co-installed with OpenCV.

B. Polar Conversion

As a first step for calculating our estimator, we remap the image to radial coordinates, using the center of the images $(x_{p,0}, y_{p,0}) = (W_0/2, H_0/2)$ as the origin of the new polar reference system. Therefore, the Cartesian images $(x,y) \in ([0,W_0], [0,H_0])$ are converted into a polar representation $(r, \theta) \in ([0, R_0], [0, \Theta_0[)$, where $R_0 = \sqrt{x_{p,0}^2 + y_{p,0}^2}$ with resolution $r_{min} = 1\,\text{px}$ and $\Theta_0 = 360°$ with resolution $\theta_{min} = 1°$. The coordinates change is accomplished using the following formulas:

$$\begin{cases} r &= \sqrt{x^2 + y^2} \\ \theta &= \arctan(\frac{y}{x}). \end{cases} \quad (4)$$

While this coordinate transformation presents some complexity in the mathematical description, it is a rigid remapping

of pixel coordinates and therefore, for a given sensor, it can be hard-coded on the microcontroller e.g., as a pre-computed indirection lookup table, with minimal impact on the computing speed. Our radial analysis is then applied to the polar representation of the image.

C. Radial Focus Analysis

As an example, we will consider synthetic images with a resolution $(W_0, H_0) = (1366, 1366)\,\text{px}$. In order to analyze the focus behavior as a function of the radius r, we use a 16-spoke Siemens star target, which is a standard testing target for optical instruments, as it presents a radial symmetry, and as defocusing is not affected by astigmatism (Fig. 1). The radial analysis consists in applying the Laplacian-variance
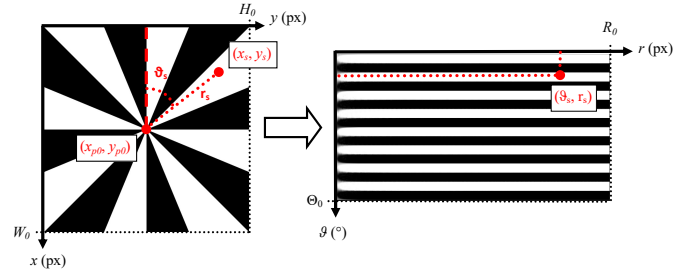

Fig. 1. On the left it is represented a 16 Spokes Siemens star target of size (W_0, H_0) with the corresponding Cartesian reference system (x, y). The point (x_{p0}, y_{p0}) represents the origin of the new polar reference system. Given a generic point (x_s, y_s) in the Cartesian reference system, the equivalent polar coordinates after the conversion are (θ_s, r_s). On the right, it is shown the polar representation of the reference target, where the same (θ_s, r_s) point is represented in the polar plane.

method to $1\,\text{px}$ annular sections of the Siemens target starting from the image center up to the borders. Thanks to the polar transformation, this can be performed applying Eq. 2, which effectively becomes a unidimensional second derivative, to the different $1\,\text{px}$ width columns of the polar representation of the image, calculating then the variance over the column. The result represents the local annular variance of the target as a function of the image radius (Fig. 2), which is our metric for evaluating the image's local focus along the radial direction.

The resulting Laplacian variance represents the highest obtainable reference value when considering a (W_0, H_0) size image of a 16-spoke Siemens star target. This constitutes a reference value for focus map evaluation when considering experimentally acquired images of the same 16-spoke Siemens star target. It is possible to notice a very steep drop of the Laplacian variance when moving to the image center ($Radius \to 0$), mainly due to interpolation error when performing the polar conversion. Therefore, the radial focus analysis results are reliable only where the Laplacian variance of the reference image stabilizes to a constant value, in practice for $Radius > 150px$.

D. Local Annular Gaussian Defocus Analysis

To understand the behavior of this estimator ahead of an experimental evaluation on real-life images, we examined the
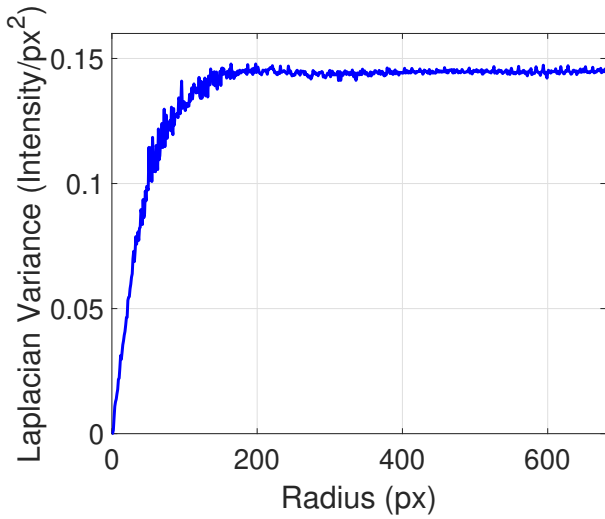
Fig. 2. The plot represents the radial Laplacian variance of a (W_0, H_0) PNG image generated from a vector graphics reference Siemens target. The Laplacian variance is computed for each column of the image polar representation (Fig. 1), which provides an indication of the image degree of focus as a function of the radius (px).

Laplacian variance changes when applying a defined amount of defocus in an annular section of the reference Siemens target image. The defocus is introduced in annular sections ranging from $R_{d,min} < Radius < R_{d,max}$ using a Gaussian blur operator with a specific kernel size. Fig. 3 reports the
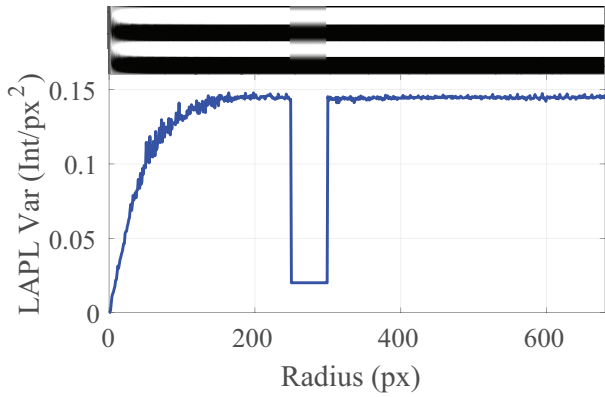

Fig. 3. In the upper part we show a fraction $(\theta \in [3/4 \cdot \Theta_0, \Theta_0])$ of a 16-spoke reference target in polar coordinates, where a Gaussian defocus with a kernel size $(k, k) = (11, 11)$ is applied to the annular section corresponding to $R_{d,min} = 250$ px and $R_{d,max} = 300$ px. The plot below is aligned to the image to appreciate better the sudden drop in the radial Laplacian Variance in correspondence to the applied Gaussian defocus.

reference Siemens target image in polar coordinates with a Gaussian defocus applied between $R_{d,min} = 250$ px and $R_{d,max} = 300$ px with the correspondent Laplacian variance as a function of the radius. The Gaussian blur, with (k, k) kernel size, is directly applied to the polar representation of the target. As expected, the Laplacian variance presents a drop in correspondence to the applied defocus region. In order to correlate the amount of applied defocus to this drop, it is useful to plot the normalized Laplacian variance of the defocused

region as a function of the Gaussian defocus kernel (Fig. 4). As reasonably expected, the normalized Laplacian variance
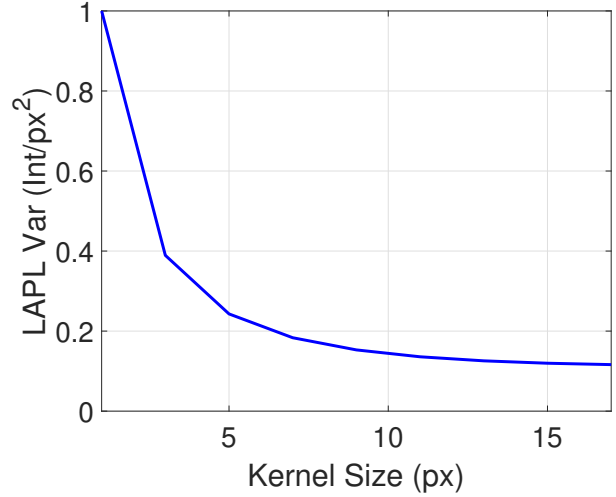

Fig. 4. The plot represents the normalized Laplacian Variance computed in Gaussian blurred regions as a function of the Kernel size.

value shows to be unitary when the kernel is $(k, k) = (1, 1)$ and decreases as the kernel size increases.

E. Computational Complexity Evaluation

The described radial focus evaluation method is proposed as a lower computational complexity alternative to standard Laplacian-based approaches. For comparison, in the following, we summarize the processing steps for both approaches.

The standard Laplacian method consists of 1,a) calculating the Laplacian (Eq. 1) of the overall image (W_0, H_0) in Cartesian coordinates and 1,b) computing its variance over annular regions concentric to the image center. The proposed approach consists instead of: 2,a) Cartesian-to-polar coordinate conversion of the image, 2,b) computing the mono-dimensional Laplacian for each column of the polar image, 2,c) calculating the variance of each column of the Laplacian.

The computational complexity can be evaluated as the number of required sum, product, and division operations. In particular, the computational cost for each computational step is summarized in Table I. As can be seen from Table I, the only additional phase required in the proposed approach is the conversion to polar coordinates. However, as detailed in section III.b, this contributes to minimal computational effort, since it can be hard-coded. Therefore, the effective computational contribution can be attributed only to the Laplacian computational and variance computational phases of both approaches.

The core improvement in computational cost is exhibited by the Laplacian computation. Indeed, in the standard case, the Laplacian can be computed using central differences, by convolution with a 3x3 Kernel (9 sums and 9 products), whereas in the proposed approach the central differencing scheme is applied using a 3x1 Kernel (3 sums and 3 products).

Standard Laplacian Approach				
Algorithm Phase	**Computational Cost**			
	Products	Sum	Division	N° exec.
Laplacian Compute	9	9	0	$W_0 \cdot H_0$
Variance Compute — Summation	3	1	0	$W_0 \cdot H_0$
Variance Compute — Normalization	0	0	1	$H_0/2$
Proposed Radial Laplacian Approach				
Algorithm Phase	**Computational Cost**			
	Products	Sum	Division	N° exec.
Polar Conversion	0	0	0	$W_0 \cdot H_0$
Laplacian Compute	3	3	0	$W_0 \cdot H_0$
Variance Compute — Summation	3	1	0	$W_0 \cdot H_0$
Variance Compute — Normalization	0	0	1	$H_0/2$

TABLE I

SUMMARY OF THE ELEMENTARY OPERATIONS (SUM, PRODUCT, AND DIVISION) REQUIRED FOR ALL THE COMPUTATIONAL STEPS OF BOTH STANDARD LAPLACIAN AND OUR PROPOSED RADIAL LAPLACIAN APPROACHES

As a matter of fact, the computation of the variance can be optimized applying certain precautions. In particular, if adopting a zero-mean kernel for the Laplacian computation, it is possible to avoid 1 sum and 1 product operation to the summation phase, since we avoid the subtraction of the mean from the Laplacian (Eq. 1). Also, the only division necessary to compute the variance can be reduced to a simple bit shift if a power of 2 number of pixels is chosen on each annulus. As a result, the computational complexity contribution of the single algorithms is dominated by the computation of the Laplacian, which indeed is significantly lighter in our approach.

As a representative example, on our images of resolution $(W_0, H_0) = (1366, 1366)$ px, the standard Laplacian approach offers an overall computational complexity of $(N_{sum}, N_{prod}) = (9, 11) \cdot W_0 \cdot H_0 \approx (16793604, 20525516)$; on the other hand, our proposed radial Laplacian approach offers an overall computational complexity of $(N_{sum}, N_{prod}) = (3, 5) \cdot W_0 \cdot H_0 \approx (5597868, 9329780)$.

IV. EXPERIMENTAL MEASUREMENTS AND RESULTS

In this section, the proposed radial focus evaluation algorithm is applied to experimentally acquired images. For a proper comparison with the theoretically obtained data, a printed 16-spoke Siemens target has been used. In section IV-A, the imaging setup used to acquire experimental images is presented, in section IV-B, the measuring protocol together with a pre-processing phase used to evaluate the best focus condition is described, and in section IV-C, the radial focus evaluation algorithm is applied to the experimental data.

A. Measuring Setup

The measuring system is based on a standard imaging setup placed in front of the reference image at a distance $D = 50\,\text{mm}$ (Fig. 5). The target is illuminated using a monochromatic light ($\lambda_0 = 480\,\text{nm}$ - $\Delta\lambda_{FWHM} = 10\,\text{nm}$) directed at the target center using an optical fiber bundle. The acquisition system is composed of a monochrome CMOS camera (GS3-U3-32S4M-C, Teledyne FLIR LLC, UK), a 23

mm objective lens (Xenoplan 23-0902, Schneider Kreuznach GmbH, Germany) and a tunable liquid lens (EL-16-40-TC-VIS-5D-M30.5, OptoTune AG, Switzerland) placed on the objective filter mount. The system is based on a hyperspectral imaging setup developed by our research group [11].
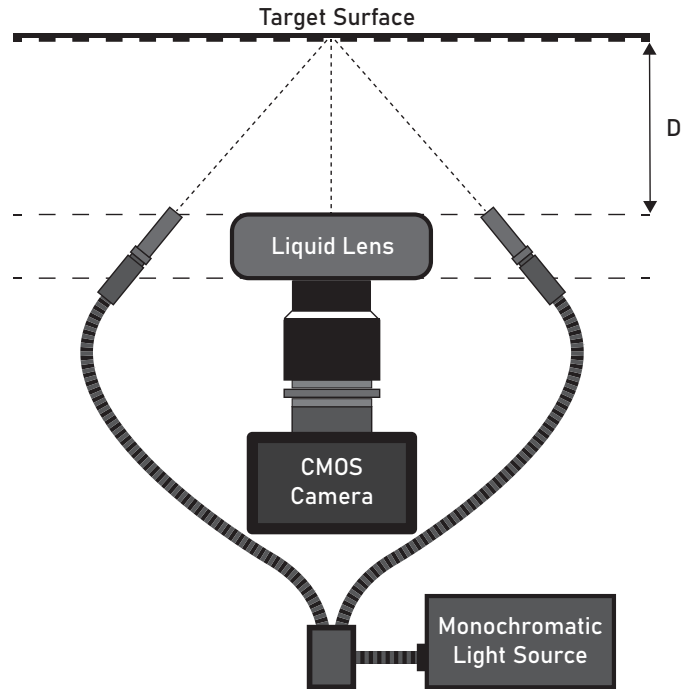

Fig. 5. Schematic representation of the measuring system.

The CMOS camera is set up to acquire grey scale PNG images with 1824x1366 px resolution.

B. Measuring Protocol and Global Focus Optimization

The imaging system is placed in front of a 16-spoke Siemens target, whose center is qualitatively positioned to appear at the camera sensor center. The optical system is designed to present a focal plane placed at a distance approximately $5\,\text{mm}$ from the liquid lens' last surface. Initially, the liquid lens is set to a zero-diopter correction. The imaging system is then positioned by the user to qualitatively obtain the best image focus level. The liquid lens optical power is then scanned from $-1\,\text{D}$ to $+1\,\text{D}$ in steps of $0.02\,\text{D}$ and target images for each correction value are acquired. For a comparison with theoretical data, all acquired images are cropped to a square form factor that shares the same resolution $(1366, 1366)$ px as the reference target images.

To baseline the proposed radial focus estimation to the correct scan image, the liquid lens focal power correction required to obtain the best overall image focus is found using the standard Laplacian estimation, by calculating the Laplacian of the full image, thus identifying the image with the highest overall variance of this Laplacian.

C. Experimental Radial Laplacian Variance

The radial focus estimation algorithm described in Section III is applied to all the acquired images. The experimental

radial Laplacian variance as a function of the image radius is shown in Fig. 6. It is possible to appreciate that the radial Laplacian variance, corresponding to the previously determined image with the highest overall focus, returns also a locally higher radial focus value with respect to all other images for all radius values.
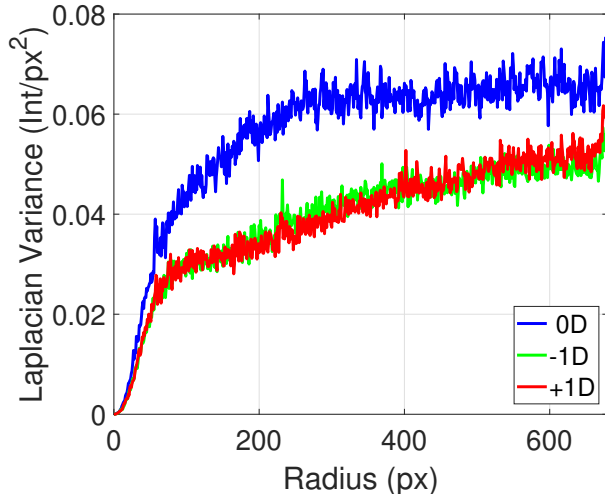

Fig. 6. Experimental radial Laplacian variance as a function of the image radius. The blue curve represents the image corresponding to the higher overall degree of focus, which is related to a specific focus correction of the liquid lens. The red and green curves represent the images when applying a defocus of +1D and −1D respectively with respect to the condition of highest focus. As expected, the Laplacian variance is lower as the image degree of focus decreases.

V. CONCLUSIONS

The development of focus estimation metrics with high speed and low computational complexity is fundamental when designing compact and portable ophthalmic imaging devices, where the auto-focus algorithm can rely only on the information given by the image acquired by the sensor and on the processing power of low-cost and low-power electronics (e.g. inexpensive microcontrollers). This is a typical case encountered in portable ophthalmic imaging devices. The focus metric proposed in this paper is capable of estimating the focus of annular sections of the imaging area. Exploiting radial symmetry, the proposed focus estimation shows a reduced computational complexity when compared to standard Laplacian-based focus estimation approaches.

This paper is intended to present a focus estimation operator with low computational complexity, which is only an element of a complete auto-focusing algorithm for ophthalmic instrumentation. Indeed, the next immediate phase in the development of this project will need to address i) the evaluation and optimization of experimental computation time/complexity, which up to now has been only theoretically estimated, ii) the evaluation of the performance using a target more representative of ophthalmic images, as the present target cannot be defocussed in the radial direction and thus does not account for astigmatism.

More prospectively, the current state of the proposed focus estimation procedure does not allow for a comprehensive evaluation of its dynamic range, and of its robustness to noise and artifacts. However, these factors are essential considerations in the assessment of any focus estimation method and, as such, they represent an important step to applicability in real-life situations. In our future studies we will therefore need to address the performance of the proposed technique, through modeling and appropriate experimental work, evaluating its dynamic range with respect to defocus and to image characteristics, its robustness in the presence of noise and out-of-plane artifacts, such as those commonly encountered in ophthalmology, and to examine eventual further use-specific limitations.

REFERENCES

[1] J. Knapper, J. T. Collins, J. Stirling, S. McDermott, W. Wadsworth, and R. Bowman, "Fast, high precision autofocus on a motorised microscope: automating blood sample imaging on the OpenFlexure Microscope," Sep. 2021, [Online; accessed 22. Nov. 2022]. [Online]. Available: https://www.arxiv-vanity.com/papers/2109.06842

[2] C.-P. Chiu, T.-J. Chiang, J.-K. Chen, F.-C. Chang, F.-H. Ko, C. W. Chu, S.-W. Kuo, and S.-K. Fan, "Liquid Lenses and Driving Mechanisms: A Review," *J. Adhes. Sci. Technol.*, vol. 26, May 2012.

[3] M. Menolotto, I. A. T. Livingstone, and M. E. Giardini, "An Imaging-based Autorefractor," in *2021 IEEE International Instrumentation and Measurement Technology Conference (I2MTC)*, May 2021, pp. 1–6, iSSN: 2642-2077.

[4] B. Amirsolaimani, G. Peyman, J. Schwiegerling, A. Bablumyan, and N. Peyghambarian, "A new low-cost, compact, auto-phoropter for refractive assessment in developing countries," *Scientific Reports*, vol. 7, no. 1, p. 13990, Oct. 2017. [Online]. Available: https://www.nature.com/articles/s41598-017-14507-5

[5] "Vision-R 700 Auto Phoropter." [Online]. Available: https://www.essilorinstrumentsusa.com/products/exam-room/vision-r-700/

[6] Y. Sun, S. Duthaler, and B. J. Nelson, "Autofocusing in computer microscopy: selecting the optimal focus algorithm," *Microsc. Res. Tech.*, vol. 65, no. 3, pp. 139–149, Oct. 2004.

[7] S. Pertuz, D. Puig, and M. García, "Analysis of focus measure operators in shape-from-focus," *Pattern Recognit.*, vol. 46, Nov. 2012.

[8] J. L. Pech-Pacheco, G. Cristobal, J. Chamorro-Martinez, and J. Fernandez-Valdivia, "Diatom autofocusing in brightfield microscopy: a comparative study," in *Proceedings 15th International Conference on Pattern Recognition. ICPR-2000.* IEEE, Sep. 2000, vol. 3, pp. 314–317vol.3.

[9] G. Bradski, "The OpenCV Library," *Dr. Dobb's Journal of Software Tools*, 2000.

[10] C. R. Harris, K. J. Millman, S. J. van der Walt, R. Gommers, P. Virtanen, D. Cournapeau, E. Wieser, J. Taylor, S. Berg, N. J. Smith, R. Kern, M. Picus, S. Hoyer, M. H. van Kerkwijk, M. Brett, A. Haldane, J. F. del Río, M. Wiebe, P. Peterson, P. Gérard-Marchant, K. Sheppard, T. Reddy, W. Weckesser, H. Abbasi, C. Gohlke, and T. E. Oliphant, "Array programming with NumPy," *Nature*, vol. 585, no. 7825, pp. 357–362, Sep. 2020. [Online]. Available: https://doi.org/10.1038/s41586-020-2649-2

[11] L. Di Cecilia and L. Rovati, "Design and performance of a hyperspectral imaging system: Preliminary in vivo spectral reflectance measurements of the human iris," *Rev. Sci. Instrum.*, vol. 91, no. 1, p. 014104, Jan. 2020.